International Journal of Applied Earth Observation and Geoinformation 129 (2024) 103776

Contents lists available at ScienceDirect

International Journal of Applied Earth Observation and Geoinformation

journal homepage: www.elsevier.com/locate/jag

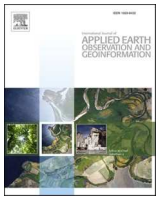

L-band microwave-retrieved fuel temperature predicts million-hectare-scale destructive wildfires

Ju Hyoung Lee [a,*], Sander Veraverbeke [b], Brendan Rogers [c], Yann H. Kerr [d]

[a] Univ. of Guelph, H.L. 50 Stone Rd E, Guelph, ON, Canada
[b] Faculty of Science, Earth and Climate, Vrije Universiteit Amsterdam, Amsterdam, Netherlands
[c] Woodwell Climate Research Center, 149 Woods Hole Road, Falmouth, MA, USA
[d] 18 Av. Edouard Belin, Toulouse 31401 Cedex 09, France

ARTICLE INFO

Keywords:
Fire fuel temperature
Vegetation heat
Large-scale wildfires
Amplifying effects
Passive microwave sensors

ABSTRACT

The 2014 Northwest Territories fires are one of the largest wildfires in history. However, it is difficult to explain what caused such devastating wildfires simply with meteorological conditions and hydrological drought. There is a lack of large-scale Near-Real-Time (NRT) observations that characterize fuel conditions. To fill this research gap, we provide the new earth observations that the *meso*-scale vegetation heat represented by L-band microwave-retrieved fuel (or canopy) temperature serves as a predictor of fire spread and lightning. We studied two million-ha-scale extreme fire events in the Northwest Territories in 2014 and British Columbia in 2018 to demonstrate that preheated endothermic vegetation condition (canopy temperature>295 K) ahead of flaming is a prerequisite for mega-fires. Canopy temperature is thus proposed as an indicator to modulate convective heating ahead of combustion, and fire spread, which strongly correlated (R^2 of 0.8 ~ 0.9) with pre-fire canopy temperature increments. It is possible to predict large-wildfires with this threshold of canopy temperature. We suggested a mechanism for vegetation under heat stress to trigger ignition and spread large fires. Our findings provide additional evidence that continued warming of the Earth's surface will lead to more severe firestorms and carbon emissions.

1. Introduction

Boreal forests are the largest intact forest biome in the world (Wells et al., 2020), with a large fraction within Canada. Boreal forests exert a significant influence on global climate, largely owing to their high terrestrial carbon storage, and characteristic surface albedo as well as surface energy budgets (Bonan, 2008; Flannigan, 2015; Jones et al., 2022). The climate is warming considerably faster in high-latitude regions compared to other places on Earth, leading to the intensification of boreal fire regimes (Bradshaw and Warkentin, 2015; Walker et al., 2019). Considering that destructive fires started from only ~ 3 % of the total area burned, fire spread is severe, especially in Canada. Given the recent increases in fire frequency and burned area, there is a growing consensus that more attention needs to be paid to fuel continuity and accumulation rather than facing the limits of our ability to suppress fire events (Moore, 2019). In particular extreme mega-fire disasters will have a huge impact on environmental quality and carbon emission and generate subsequent firestorms as a chain reaction.

The chain reaction occurs due to the overarching impact of drying land surface on the atmosphere. Several studies have shown that mesoscale land surface such as vegetation cover often promotes deep convection, triggering lightning or storm that ignites and/or exacerbates wildfires (Chen et al., 2021; Taylor et al., 2012; Taylor et al., 2011; Wang et al., 2009). Vegetation condition plays a more important role in generating deep convection as compared to synoptic atmospheric conditions during weak flow (i.e., wind speeds less than 10 m/s at 500 hPa) (Carleton et al., 2008). Given that boreal forests have higher sensible heat fluxes than tundra (Dissing and Verbyla, 2003; Flannigan, 2015), such convective heat and dry fuels in coniferous boreal forests are likely to intensify fire severity, and fire-nados (Lareau et al., 2018; Nauslar et al., 2018; Zhang et al., 2019). Early prediction of fire severity especially firestorms is therefore of paramount importance for fire management.

Despite such an amplifying impact of vegetation (Chen et al., 2021; Yebra et al., 2013), the most widely-used wildfire prediction systems are based purely on weather forecast information (van Wagner, 1987).

* Corresponding author.
E-mail address: ju.lee@mail.com (J.H. Lee).

https://doi.org/10.1016/j.jag.2024.103776
Received 15 November 2023; Received in revised form 6 February 2024; Accepted 17 March 2024
Available online 29 March 2024

Among the challenges for predicting the severity of large-scale wildfires is the lack of availability of Near-Real-Time (NRT) live fuel information on vegetation dynamics for use in operational decision-making. In response to this scarcity of fuel information, there have been many attempts to use satellite observations for monitoring vegetation conditions. However, there are several limitations in applying satellite observations for wildfires (Leblon et al., 2012; Leblon 2016). Satellite-based Normalized Difference Vegetation Index (NDVI) and differenced Normalized Burn Ratio (dNBR) have been used to determine live fuel moisture or burn severity (Parks et al. 2014; Yebra et al. 2013; Yebra et al. 2022). However, NDVI is a better predictor of vegetation chlorophyll content than live fuel moisture(Ceccato et al., 2001; Chen et al., 2021; Leblon, 2005). Thermal infrared images are used to estimate land surface temperature or energy balance-based estimates of evapotranspiration. Land surface temperature exhibits a better relationship with fire weather indices or fuel moisture than NDVI (Leblon, 2005). Nolan et al. (2016) attempted to estimate dead fine fuel moisture content (FM) from Moderate Resolution Imaging Spectroradiometer (MODIS) land surface temperature. Nonetheless, it has several limitations for operational implementation, including that optical or thermal infrared images are largely affected by cloud shadows. Additionally, land surface temperature estimates do not take into account the heat transfer from leaves, and are not sensitive to moisture fluctuations (Leblon, 2005). When using it for evapotranspiration as a proxy of vegetation moisture, there is an impediment. Live vegetation moisture is much less dependent on atmospheric conditions than dead vegetation because it is more dependent on soil moisture(Szpakowski and Jensen, 2019). For fire severity, MODIS Fire Radiative Power is often used as a measure of biomass consumption in fire. However, only 15 ~ 30 % of the total heat energy contributes from radiation, implying that convective fire energy, a majority of combustion is not included(Dickinson et al., 2016). Finally, the backscatter observed from the European Remote Sensing satellite (ERS)-1/-2 Synthetic Aperture Radar and RADARSAT-1/-2 have been used for post-fire management (Pirotti et al., 2023; Szpakowski and Jensen, 2019). However, C-band backscatter is influenced by confounding factors such as surface roughness and volume scattering from vegetation and is less able to penetrate the forests than L-band microwaves.

L-band microwave observations are certainly more effective for monitoring the moisture of vegetation. As compared to thermal infrared or C-band microwave sensors, L-band radiometry has several advantages for characterizing vegetation fuel conditions. That includes the semi-transparence of the vegetation layer, reduced scattering signals within the vegetation canopy, and a reduced influence from soil roughness on the microwave measurements (Meyer et al., 2018). Radio frequency interferences (RFI) and atmospheric effects such as rain or storms are also comparatively limited at this frequency(Reul et al., 2016).

In this study, we propose a methodology to predict mega-fires at the incipient stage of fire development, which may ultimately enhance fire management. To this end, we employed a space-borne L-band microwave radiometer to estimate canopy temperature. Canopy temperature is used as a proxy for indicating *meso*-scale fuel dryness required to predict when and where mega-fires will spread, as it provides information on the progress of dehydration of preheated endothermic vegetation before combustion occurs. This measure was applied to two mega-fire events in western Canada, in which more than 4.9 M ha of boreal forest burned.

More importantly, we provide a conceptual breakthrough in the application of satellite data from the detection of ongoing or post-fire events using SAR or thermal infrared images to predict ahead of combustion. In this respect, this approach is set apart from traditional satellite data applications, which detect smouldering or flame as an exothermic product of combustion.

2. Methods

2.1. Study area

The Northwest Territories (NWT; June to October 2014) and British Columbia (BC; July to November 2018) experienced mega-fires that burned 3.5 million ha (94.3 Tg C) and 1.35 million ha, respectively (Fig. 1) (Veraverbeke et al., 2017; Walker et al., 2018; Wang and Strong, 2019). The 2014 fire season in the NWT was the highest in terms of area burned. The 2018 fire season was the largest on record in BC in terms of area burned since 1950 when modern records began.

These areas were exposed to drying conditions during and before the wildfire event (Kochtubajda et al., 2019). The hydrometeorological data shows that the monthly discharge for the La Martre River below the outlet of Lac La Martre (station ID: 07TA001, please see https://api.weather.gc.ca/collections/hydrometric-stations/items/07TA001 for the location) decreased from 37.5 m^3/s in June to 29.1 m^3/s in July and 24.3 m^3/s in August 2014(ECCC, 2022). At Yellowknife (climate ID: 2204101), daily rainfall was almost zero from May 28 to July 29, except for two rain events at 4 mm. Daily mean air temperature during the same period ranged between 6 and 22 °C. During mid-June and July, a daily wind speed of maximum gust ranged from 35 to 55 km/h. For a comparison between fire and no-fire years, the monthly discharge for La Martre river outlet was higher at 50 ~ 65 m^3/s in 2013, 2018, and 2020 with no fires. Daily rainfall was similarly zero, except for 3 ~ 4 rain events at 10 mm during the same season in 2013, and 2020, while there were several rain events at greater than 10 mm in 2018. Air temperature was similar to 2014, ranging between 8 and 22 °C during the same season in 2013, 2018 and 2020. A daily wind speed of maximum gust was similar to 2014, ranging from 35 to 55 km/h in 2013, 2018, and 2020 as well. For climatological anomalies, please see Kochtubajda et al. (2019).

Around fire-affected areas in BC, the monthly discharge for Dean River below Tanswanket Creek (08FC003, see https://api.weather.gc.ca/collections/hydrometric-stations/items/08FC003 for location) dropped from 23.5 m^3/s in June to 9.78 m^3/s in July and 3.48 m^3/s in August 2018. At Ootsa Lakeskins Lake (climate ID: 1085836), daily precipitation was almost zero from July 9 to September 1, except for one rain event at 9 mm. Daily mean air temperature during the same period ranged between 10 and 20 °C. During mid-July and August, a daily wind speed of maximum gust was between 35 and 45 km/h.

Cloud-to-ground lightning data was obtained from the Canadian Lightning Detection Network (CLDN) (Orville et al., 2011). Polygon data for fire-affected areas and point data for ignition were acquired from the Canadian National Fire Database (CNFDB)(Canada, 2022).

2.2. Retrieval of canopy temperature

Canopy temperature is closely related to sensible heat as follows (Kustas and Norman, 1997):

$$H_c = \rho Cp \frac{T_c - T_a}{R_a} \quad (1)$$

where H_c is vegetation sensible heat flux (W/m^2), ρ Cp is the volumetric heat capacity of air (J/m^3 K), T_c is canopy temperature (K), T_a is the air temperature at some reference height above the surface (K), and R_a is the resistance to heat transport (s/m). For gradient temperatures that should be informed to characterize sensible heat, canopy temperatures were assumed sufficient because of the endothermic ability of vegetation and the poor conductibility of air as a heat sink (Oehri et al., 2022). Especially in drying conditions such as preheated fuels ahead of flame, canopy temperature is higher than air temperature (Luan and Vico, 2021). In the event of rain, it is observed that air temperature suddenly drops during wildfire spread, generating a bigger increment between canopy and air temperature. Thus, canopy temperature is key for

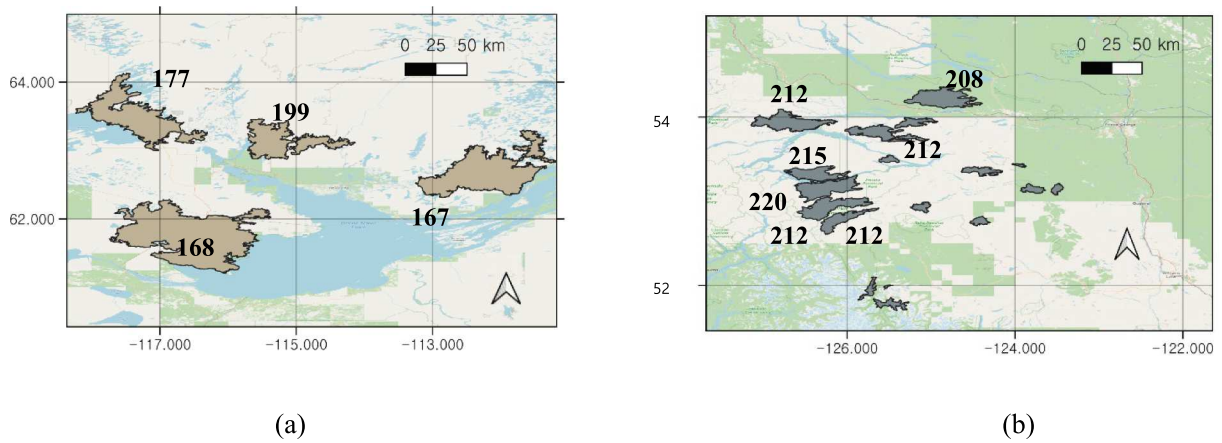

Fig. 1. Location of the megafires considered in this study: (a) 2014 wildfires in NWT (b) 2018 wildfires in BC. The number shows ignition dates in Day of Year (DoY). Background map came from open street map.

inferring vegetation heat, as air temperature usually fluctuates below canopy temperature.

Canopy temperature is also an essential element in the fire spread mechanism. To sustain flaming combustion, fuels release heat and volatiles through pyrolysis. This is governed by the energy balance between the fuel preheating such as convective heating over the top surface of the fuel or convective heating within the fuel bed, and the heat needed to release volatiles as follows (Liu et al., 2021).

$$Q_s = m\left(H_g + c_p\left(T_f - T_{air}\right)\right) = Q_{net} \quad (2)$$

where, Q_s denotes the heat needed for pyrolysis that releases volatiles, m is the mass burning rate, H_g is the heat of gasification, c_p is the average specific heat of the fuel, T_f is the fuel temperature, T_{air} air temperature, Q_{net} is the net heat feedback. Here, fuel temperature corresponds to canopy temperature over forests. The temperature increase of the fuels increases Q_s as well as Q_{net}. This pre-heating (pre-ignition) mechanism is accompanied by dehydration of fuels.

The canopy temperature is estimated from the L-band SMOS/SMAP brightness temperature (Lee, 2021). Microwave satellite-measured brightness temperature contains a radiation component of the canopy emission scattered at the surface and attenuated through the canopy and atmosphere, in addition to the soil emission attenuated by the canopy and atmosphere (Kerr et al., 2012). Theoretically, the 1.4 GHz L-band microwave (with a wavelength of 21 cm) penetrates more deeply through a thick vegetation layer than C-band (4 to 8 GHz), X-band (8 to 12 GHz), and Ku-band (12 to 18 GHz) beam. Specifically, L-band microwave radiometers are known to penetrate to several centimeters in soil depths (penetration depth depends on soil moisture and texture) covered by vegetation with a vegetation water content of up to 5 kg/m^2 (Liu et al., 2018). Because dense forests usually have a vegetation water content of greater than 5 kg/m^2, it is thought that the L-band satellite senses brightness temperature mainly from the top crown (e.g. leaves, needles, twigs and branches) and trunk of vegetation canopy rather than of the soil reflectivity (Link et al., 2018). In the case of dense forests, soil contribution is negligible and scattering albedo ω is almost zero (0.03 ~ 0,06), meaning that it'sextinction due to absorption (Wigneron et al., 2017). The zeroth-order τ -ω model widely used for retrieving soil moisture does not account for multiple volume scattering microwave effects or the complexity of the effects of the vegetation structure, causing lots of error propagation to estimation of vegetation optical depth (Wang et al., 2023).

First, the directional radiometric surface temperature T_R is estimated from SMOS and SMAP brightness temperature measurement T_B at view angle θ and directional emissivity ε (e.g. SMOS or SMAP brightness temperature/land surface temperature from independent sources), as follows (De Jeu and Owe, 2003; Kustas and Norman, 1997; Lee, 2021):

$$T_R(\theta) = \left\{\left[T_B(\theta)^n - (1-\varepsilon(\theta))T_{SKY}^n\right]/\varepsilon(\theta)\right\}^{1/n} \quad (3)$$

where n, the power in the Stefan-Boltzman equation, is calculated for the L-band wavelength (21 cm) and a temperature range from 190 to 315 K (Becker and Li, 1990), and the hemispherical temperature of the sky T_{sky} is 2.7 K. Atmospheric contribution at L-band is significantly small, and does not largely affect a temporal resolution of brightness temperature (Reul et al. 2012). Soil reflectivity was neglected in dense forests (Kerr et al., 2019). Then, the canopy temperature T_C is estimated from T_R.

$$T_C = \left\{\left[T_R(\theta)^n - (1-f)T_S^n\right]/f\right\}^{1/n} \quad (4)$$

where T_s is the soil surface temperature, and f is the vegetation fraction as a function of the LAI (Kustas and Norman, 1997).

2.3. Satellite data

For the NWT wildfires, the European Space Agency (ESA)'s Soil Moisture and Ocean Salinity (SMOS) Level 3 daily (version 3.3) brightness temperature product on a 25-km EASEv2 grid was acquired through the Centre Aval de Traitement des Données (CATDS) (Kerr et al., 2012). In this study, reprocessed MIR_CDF3TD products with a descending orbit were selected. For BC wildfires, the National Aeronautics and Space Administration (NASA)'s Soil Moisture Active Passive (SMAP) brightness temperature launched in 2015 with a descending orbit was obtained from Earth Data (O'Neill et al. 2021). The Level 3 radiometer data (version 5) was on a daily 9 km EASE polar grid. Surface temperature was also acquired from the same SMAP dataset.

For ancillary data, the 500 m Leaf Area Index (LAI) data was acquired from 8-day MOD15A2 Version 6 products from the Moderate Resolution Imaging Spectroradiometer (MODIS) (Myneni et al. 2015). The daily surface and soil temperature data required to calculate canopy temperature was acquired from Goddard Earth Sciences Data and Information Services Center MERRA-2 at 0.5° resolutions (GMAO, 2015).

2.4. ECMWF meteorological data

Several meteorological variables were obtained from the European Centre for Medium-Range Weather Forecasts (ECMWF) reanalysis data. Relative humidity, convective available potential energy (CAPE), and convective precipitation were acquired from 0.25° ERA5 hourly reanalysis of the Copernicus Climate Change Service (C3S) Climate Data Store, while surface sensible heat flux and evapotranspiration from vegetation were obtained from 9 km ERA5 Land hourly data (Bell et al. 2020; Hersbach et al. 2018; Muñoz Sabater, 2021). Heat flux data were collected daily at 1:00 UTC (as LST 7:00 pm on the previous day in NWT,

6 pm in BC) to separate the sensible heat emitted from wildfires from the effects of incoming solar radiation at noon. During the study period, the vegetation transpiration was low at 0.14 ~ 0.72 mm/d, while the relative humidity was around 30 ~ 50 %, and the convective precipitation was 0.03 ~ 0.38 mm/hr.

3. Results and discussions

3.1. Increments in canopy temperatures

Both SMOS and SMAP satellite-retrieved canopy temperatures appropriately represented endothermic processes of typical fire

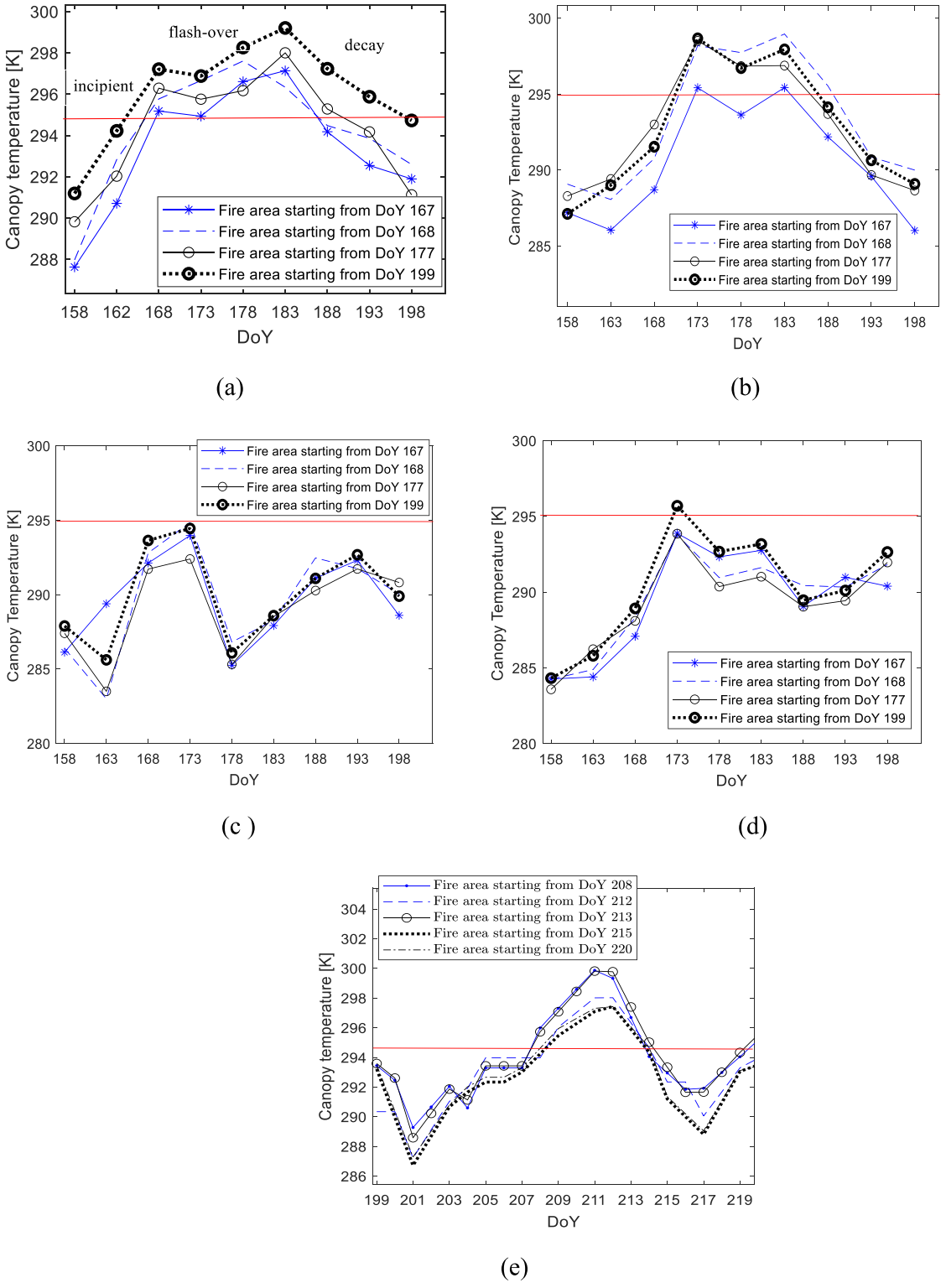

Fig. 2. Temporal evolution of the canopy temperature over burned areas: a) NWT wildfires in 2014, b) NWT wildfires in 2013, c) NWT (no fire) in 2018, d) NWT (no fire) in 2020, e) BC wildfires in 2018. Red line shows 295 K of threshold. (For interpretation of the references to colour in this figure legend, the reader is referred to the web version of this article.)

developments. In Fig. 2, canopy temperature well-differentiated fire years (>295 K) with no fire years (<295 K). The ignition occurred and fires started to spread, when exceeding a threshold of canopy temperature. As shown in Fig. 2-a, this pre-ignition phase during DoY 158 ~ 168 is referred to as the 'incipient' stage. In contrast, the post-ignition phase during DoY 168 ~ 183 is the 'flashover' stage, also called 'blow up' which makes a transit to the fires burning most vegetation with suddenly increasing fire intensity as functions of fire spread and heat release rate. At the flashover stage of canopy temperature, wildfires rapidly spread several ignitions throughout the forests as shown in Fig. 1 and Fig. 3.

Over the NWT in 2014, canopy temperatures show a non-flaming preheating phase before the ignition date on the Day of Year (DoY) 168 (Fig. 2a). At the incipient stage, with consistently increasing canopy temperature above 295 K for 10 days, desiccating vegetation is prone to ignition. At flashover, canopy temperatures exceeded 295 K, releasing heat and burning biomass. Based upon the observations of Fig. 2-a and e, the heat adsorption from a sufficient increase in canopy temperature above 295 K of a critical threshold is followed by this flashover that releases the heat. Finally, a decay stage is observed following the flashover on DoY 183. The burned areas declined along with the decrease in canopy temperature, generating small wildfires with residual heat. Although several fire events occurred on DoY 199 in Fig. 1-a, the size of the burned area was smaller at this decay stage of canopy temperature, despite a high density of lightning strikes 2 days ago (Fig. 3-c and d).

As shown in Fig. 2- c, and d, the same area under similar vegetation species and dry season with 2014 fire years did not consistently and sharply increase canopy temperature up to the level of 295 K in 2018 and 2020 when there was no fire. In 2013, the canopy temperatures sometimes exceeded 295 K during DoY 173 ~ 188, leading to small wildfires. However, they did not spread to destructive mega-fires as in 2014, due to lower fire energy (heat release) arising from small heat adsorption at the incipient stage as shown in Equation (1) and (2) (more figures will be shown later). More specifically, in Fig. 2-b, it is observed that a temperature gradient (i.e. ΔTc during DoY 158 ~ 173) and its magnitude (mostly less than 295 K) in 2013 were not as high as in 2014 when canopy temperatures continued increasing almost for a month and reaching their magnitude above 295 K while absorbing heat. For comparison in terms of burned area, 2014 wildfires with higher convective energy as functions of temperature increments, magnitudes and consequently vegetation heat spread to 1,785,000 ha during DoY 167 ~ 287. In contrast, 2013 wildfires with lower fire energy (i.e. lower preheating temperature) burned 24,591 ha during DoY 173 ~ 255.

The increment of canopy temperature before ignitions was also observed in BC wildfires. During the preheating process on DoY 201 to 210 in Fig. 2-e, canopy temperature consistently increased above a threshold of 295 K, drying fuels and absorbing heat. When reaching 300 K, fire simultaneously spread to several other areas on DoY 212, as shown in Fig. 1-b, to release heat. Although several fire events occurred on DoY 215, and 222 in Fig. 3-d, the size of the burned area was smaller at this decay stage of canopy temperature.

Because the preheating process (dehydration) of the fuels leads to pyrolysis, releasing volatiles and triggering ignition, we suggest that a large positive slope and threshold of canopy temperatures indicate fuel availability as drying vegetation fuels ahead of the flame and fire spread. Available fuels are conceptually different from the total fuels (McArthur and Cheney, 2015). Canopy temperature didn't increase when fuels

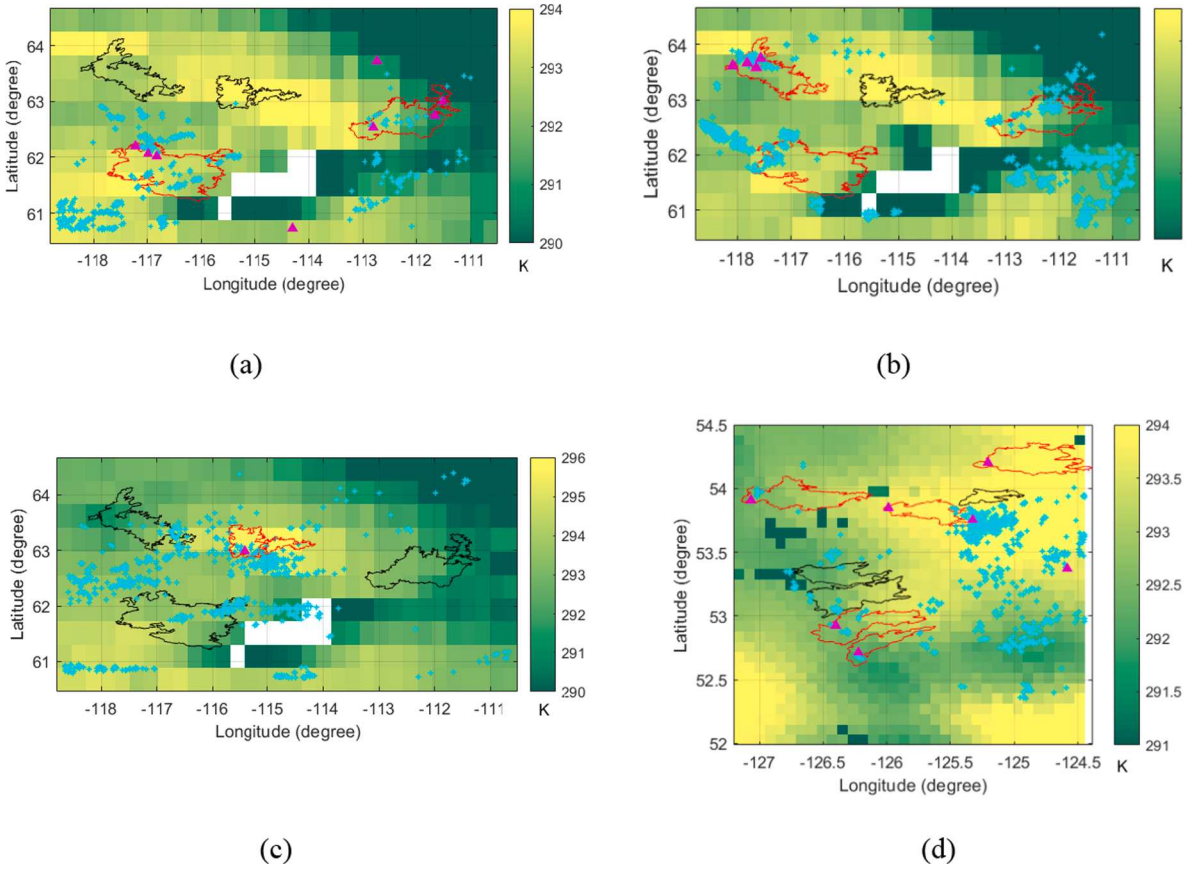

Fig. 3. Spatial distribution of 10-day averaged antecedent canopy temperatures prior to different ignition dates: a) NWT fire ignited on DoY 167b) NWT fire ignited on DoY 177c) NWT fire ignited on DoY 199, and lit on 197, d) BC fire ignited on DoY 212. Triangles ▲ represents the ignition location. Star ⋆ represents the lightning locations. Red polygons show active burning areas. Black polygons show not-ignited yet or decaying areas. (For interpretation of the references to colour in this figure legend, the reader is referred to the web version of this article.)

were not available in 2013, 2018, and 2020 in the similar dry season and vegetation species (further discussion is available at Fig. 5).

3.2. Lightning

This predictive power of drying fuels for fire spread was further scrutinized in terms of dry lightning events. In consideration of low humidity and precipitation and high canopy temperature (dry fuels) in our study areas, the lightning events were characterized as "dry" lightning, i.e. less than 2.5 mm of precipitation as defined by NOAA/NWS Storm Prediction Center (https://www.spc.noaa.gov/exper/dryt/). It is produced from heat (Kalashnikov et al., 2022; Schultz et al., 2019).

Canopy temperature is considered to have influenced lightning formation. In supplementary Fig. 1, a positive relationship between dry lightning strikes on several ignition dates and elevated antecedent canopy temperature ahead of those lightning events implies that convective heat transfer from vegetation affected lightning, and thunderstorms by producing an unstable and warm atmosphere (Chen et al., 2021; Dissing and Verbyla, 2003; Hessilt et al., 2022; Rogers et al., 2015). However, this relation is weak in BC fires, due to smaller convective heat (further discussed later).

It is difficult to explain extensive fire spread with lightning ignitions only. Over NWT and BC wildfires, as shown in Fig. 4-a and c, although dry lightning strikes were dense, the fire areas were small. In Fig. 3-d, there had been no lightning in several BC fire areas that occurred before DoY 212. Several lightning events were subsequently observed on DoY 212 in unburned areas.

Fire spread was better predicted when ignitions were combined with dry fuels than lightning ignition alone. In Fig. 4-b and d, the 10-day increments of pre-fire canopy temperature at incipient stages increased with the total burned areas at extinction stage. In Fig. 4-b and d, 'pre-fire' indicates the 10 day-averaged estimates on incipient stage during DoY 158 ~ 166 for NWT wildfires and during DoY 201 ~ 208 for BC wildfires, before all ignition occurrences. Accordingly, monitoring the pre-fire canopy temperature over ignited areas should provide predictive information on potential fire spread.

3.3. Sensible heat and fire spread

As formulated by Equation (1) and Fig. 5, canopy temperature is also related to sensible heat during the preheating process before ignitions. In Fig. 5, 'antecedent' implies the period right before various ignition events including flashover, while 'pre-fire' indicates the incipient stage before all ignitions. For example, antecedent estimates for NWT wildfires at the incipient stage correspond to a time-average of DoY 158 ~ 166 before the incipience on DoY 167 ~ 168 in Fig. 2-a, while antecedent flashover shows a time-average of 10 days right before the flashover on DoY 177. Similarly, antecedent flashover for BC wildfires takes a time average of DoY 202 ~ 211 before the flashover on DoY 212 in Fig. 2-e. Canopy temperatures at flashover and incipient stages differentiated each stage as shown by red and blue stars (fade out in the background), respectively. Surface sensible heat to be transferred upwards implies that vegetation is warmer than the air temperature.

It was found that sensible heat resulting from increased canopy

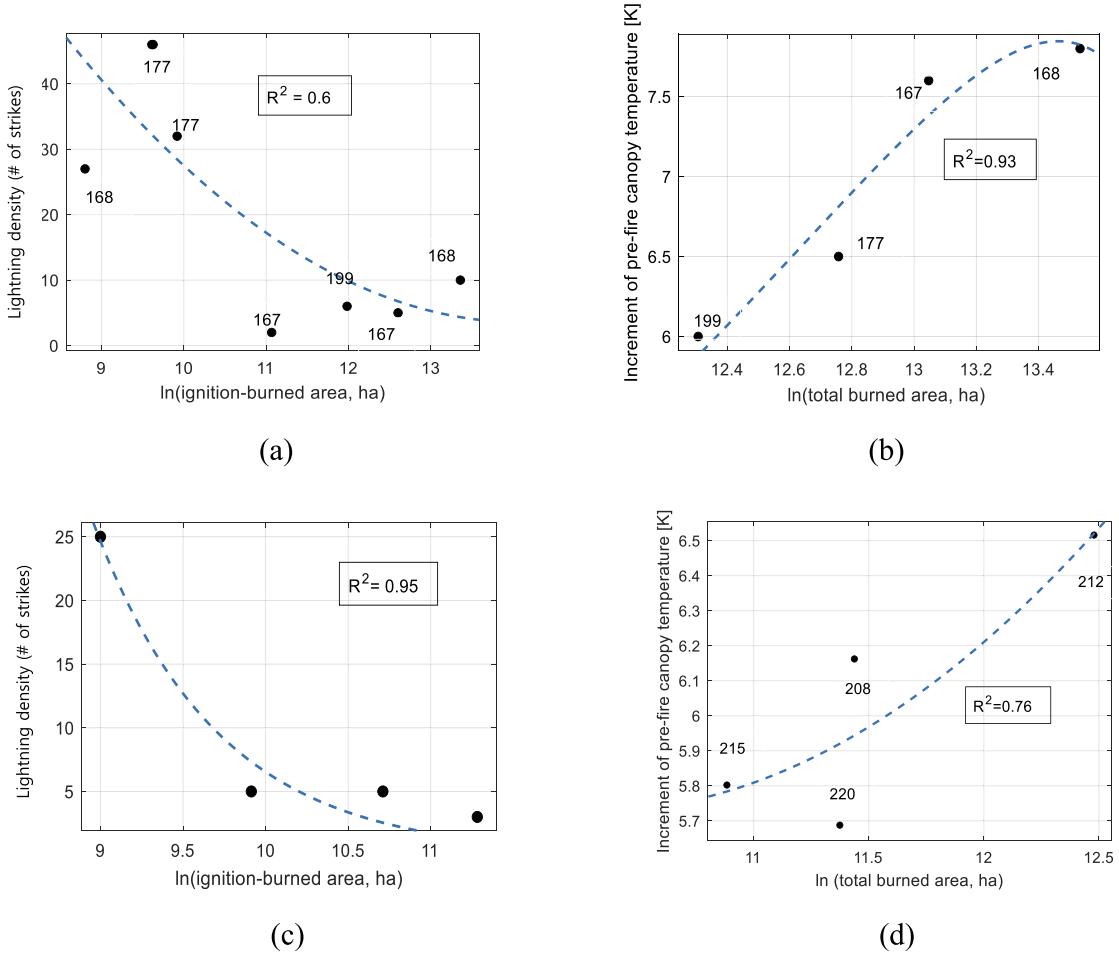

Fig. 4. Relationships with burned areas: a) lightning density over ignition points in 2014 NWT wildfires, b) 10-day increment of pre-fire canopy temperature in 2014 NWT wildfires at incipient stage, c) lightning density over ignition points in 2018 BCE wildfires on DoY 212 (there was no lightning on other ignition dates), d) 10-day increment of pre-fire canopy temperature in 2018 BCE wildfires at incipient stage. Numbers in graphs indicate ignition dates.

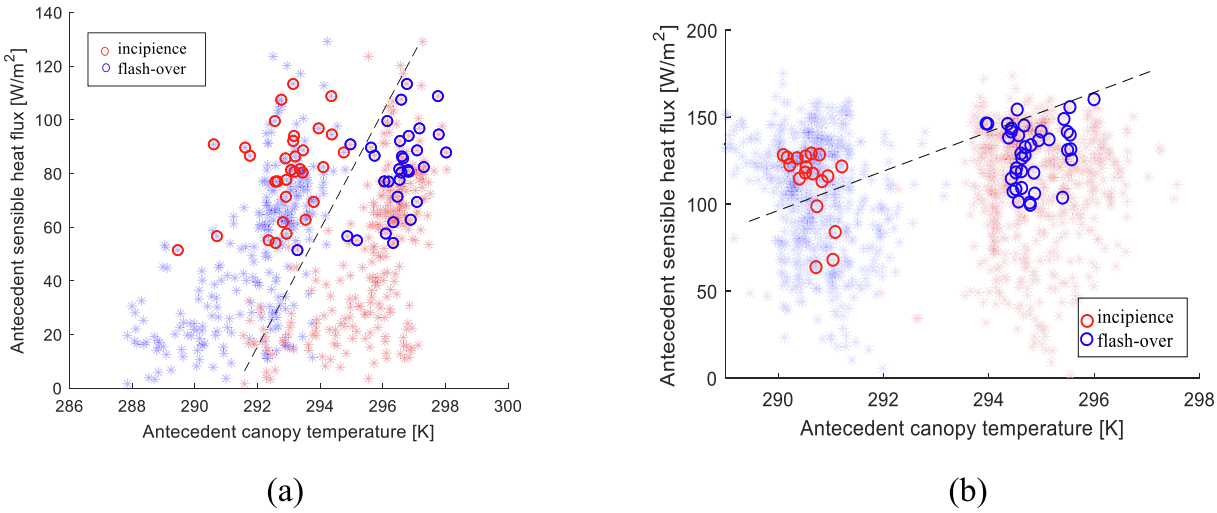

Fig. 5. Relationship between 10-day averaged antecedent upward surface sensible heat and 10-day averaged antecedent canopy temperature prior to different ignition events: (a) NWT wildfires (b) BC wildfires. Circles illustrate burned areas for each stage. Blue and red stars indicate total fuels of incipient and flash over stages, respectively. (For interpretation of the references to colour in this figure legend, the reader is referred to the web version of this article.)

temperature contributed to fire occurrence. The antecedent sensible heat in Fig. 5-a increased along with the antecedent canopy temperature, prior to both incipient and flashover stages. In particular, this correlation was more pronounced in the burned areas shown by circles than no-fire areas in the background. More specifically, sensible heat with dry fuels (i.e. higher canopy temperature) was more elevated before ignitions than that with total fuels shown by stars in the surrounding non-burned areas, suggesting the importance of identifying available fuels with canopy temperature.

In Fig. 6, temporal evolutions of higher sensible heat, and lightning strikes, as well as pre-fire canopy temperature for the NWT wildfire are well demonstrated. Negative upward sensible heat at the incipient stage decreased from −68.29 W/m^2 to −48.05 W/m^2 at flashover, implying that the preheated endothermic vegetation released sensible heat to the air by flaming. The more vegetation stores heat at the incipient stage, the more it releases heat at flashover. At the decay stage, this was recovered back to −72.45 W/m^2. Because dry lightning is also a product of convective heat, strikes also increased from 726 at the incipient stage to 1148 at flashover because a reduced upward sensible heat destabilized the atmosphere. This increase in sensible heat and lightning at flashover is reasonably well expected as antecedent the canopy temperature increased from 291.9 K to 295.555 K ahead of their increases. Thus, canopy temperatures are suggested as a good proxy to predict fire spread

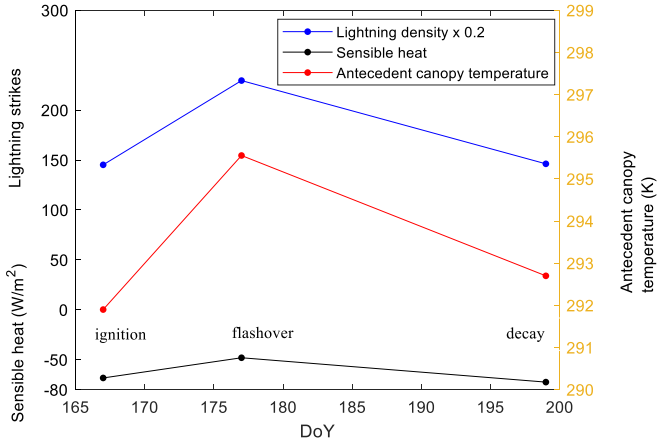

Fig. 6. Spatial average over NWT wildfires (upward sensible heat is shown by negative values).

as a function of heat adsorption (fuel dryness) and lightning ignition.

3.4. Convective energy and burned area

In addition to dry lightning and sensible heat, we also investigated how canopy temperature influenced convective energy. Vegetation-induced updraft flow against cold air deepens the atmospheric boundary layer (ABL), resulting in increases in convective available potential energy (CAPE) (Kirshbaum and Wang, 2014; Lee, 2018; Zhang et al., 2019). CAPE is highly related to the occurrence of thunderstorms or fire whirls, which leads to fast fire spread (Liu et al., 2021; Morgenstern et al., 2022).

Before ignitions, antecedent CAPE is shown to be related to antecedent canopy temperature, as shown in Supplementary Fig. 2, suggesting that both factors of canopy temperature and CAPE contributed to flashover, and that fire spread in these regions is attributed to convective heating rather than radiative energy. More specifically, in the case of NWT wildfires, the highest fire spread occurred at the incipient stage, showing the higher antecedent CAPE in red circles of burned areas. The CAPE of those areas was proportional to an increase in antecedent canopy temperature, as compared to the total fuels indicated by stars (Supplementary Fig. 2-a). Similarly, in BC wildfires, the highest fire spread occurred at the flashover stage, which exhibited higher antecedent CAPE in blue circles of flammable fuels (Supplementary Fig. 2-b). Considering its CAPE level was 10-fold smaller than NWT fires, and the gradient of canopy temperature was smaller, it can be explained why BC wildfires did not have lightning at the incipient stage. This comparison suggests that vegetation convection forces fire spread at the *meso*-scale (Carleton et al., 2008; Dissing and Verbyla, 2003).

For comparison, fire spread and burned area were not effectively captured by weather index, MODIS active fire, MODIS Fire Radiative Power, and SMAP Vegetation Water Content (VWC) in Supplementary Figs. 3-5. In Fig. 7-e, SMAP vegetation water content did not show and/or predict a vegetation dynamic as shown in canopy temperature in Fig. 2.

4. Conclusion

In this study, we explored the unknown mechanism for how warmed vegetation may trigger large-scale fires and even lightning. To discover this, we retrieved fuel (or canopy) temperature from L-band microwave sensors which can better penetrate through top crown and trunk of vegetation canopy, as compared to C-band microwave sensor. It is

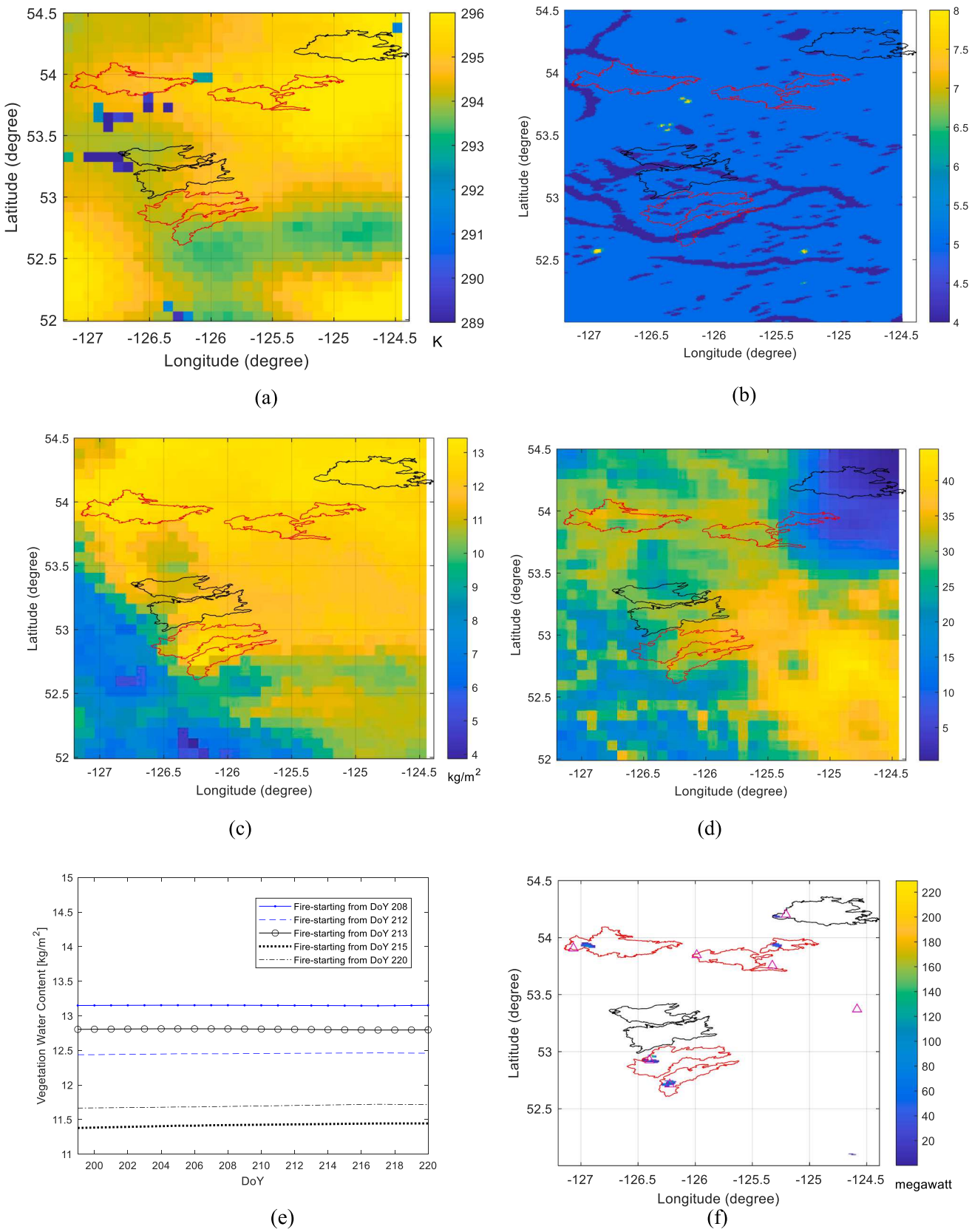

Fig. 7. Comparison with other indices over 2018 BC fires DoY 212: (a) antecedent canopy temperature (b) MODIS active fire on DoY 217 (fire occurrence is 7 of low confidence ~ 9 of high confidence) (c) fire weather index (FWI) (d) SMAP vegetation water content. (e) temporal evolution of SMAP vegetation water content (f) MODIS Maximum Fire Radiative Power on DoY 217 (triangle shows ignitions). Red polygons show active burning areas. Black polygons show not-ignited yet or decaying areas.

transparent under the cloud or smoke covers. We found that preheated endothermic vegetation condition (>295 K) ahead of flaming is a prerequisite for mega-fires. It is thus proposed to monitor a tipping point when canopy temperature exceeds 295 K and initiates convective heating to predict combustion, and fire spread.

Our findings call attention to the need to include the earth observations of canopy temperature as fuel conditions in fire prediction systems to account for vegetation heat transfer. If monitoring canopy temperatures around ignition points, fuel availability and accordingly fire spread can be estimated and used for developing an early warning system and preventing subsequent ecological damages from mega-fires.

This approach does not require to specify vegetation species and is not limited to specific vegetation species locally observed. In addition, this does not need the synoptic scale weather information obtained from interpolating several local stations. Accordingly, this approach could be applied to a global prediction system. However, there is a caveat in applying this approach. If land cover is not dense forests, then a contribution from soil reflectivity may need to be considered when retrieving canopy temperature. For future studies, we suggest applying a similar approach to other mega-fires-affected regions with different vegetation densities and structures to assess whether vegetation properties can affect convective heat and fire spread of geographical patterns.

CRediT authorship contribution statement

Ju Hyoung Lee: Conceptualization, Data curation, Formal analysis, Investigation, Methodology, Project administration, Resources, Software, Supervision, Validation, Visualization, Writing – original draft, Writing – review & editing. **Sander Veraverbeke:** Writing - review & editing, Data analysis, Investigation. **Brendan Rogers:** Writing - review & editing, Data analysis, Investigation. **Yann H. Kerr:** Writing - review & editing, Data analysis, Methodology, investigation.

Declaration of competing interest

The authors declare that they have no known competing financial interests or personal relationships that could have appeared to influence the work reported in this paper.

Data availability

Data will be made available on request.

Acknowledgement

We thank Environment and Climate Change Canada for their permission to use Canadian Lightning Detection Network data and Natural Resources Canada, Canadian Forest Service, Northern Forestry Centre, Edmonton, Alberta (https://cwfis.cfs.nrcan.gc.ca) for providing a fire weather index. This work is supported by Northern Water Futures, a project in the CFREF-funded Global Water Futures program.

Appendix A. Supplementary material

Supplementary data to this article can be found online at https://doi.org/10.1016/j.jag.2024.103776.

References

Becker, F., Li, Z.-L., 1990. Temperature-independent spectral indices in thermal infrared bands. Remote Sens. Environ. 32, 17–33.

Bell, B., Hersbach, H., Berrisford, P., Dahlgren, P., Horányi, A., Muñoz Sabater, J., Nicolas, J., Radu, R., Schepers, D., Simmons, A., Soci, C., Thépaut, J-N. (2020). ERA5 hourly data on pressure levels from 1950 to 1978 (preliminary version). Copernicus Climate Change Service (C3S) Climate Data Store (CDS). In B. Bell, Hersbach, H., Berrisford, P., Dahlgren, P., Horányi, A., Muñoz Sabater, J., Nicolas, J., Radu, R., Schepers, D., Simmons, A., Soci, C., Thépaut, J-N. (Ed.).

Bonan, G.B., 2008. Forests and climate change: forcings, feedbacks, and the climate benefits of forests. Science 320, 1444–1449.

Bradshaw, C.J.A., Warkentin, I.G., 2015. Global estimates of boreal forest carbon stocks and flux. Global Planet. Change 128, 24–30.

Canada, N.R., 2022. Canadian National Fire Database. In: Canada, N.R. (Ed.), Natural Resources Canada, Canadian Forest Service, Northern Forestry Centre. Edmonton, Alberta.

Carleton, A.M., Travis, D.J., Adegoke, J.O., Arnold, D.L., Curran, S., 2008. Synoptic circulation and land Surface influences on convection in the Midwest U.S. "Corn Belt" during the Summers of 1999 and 2000. Part II: role of vegetation Boundaries. J. Clim. 21, 3617–3641.

Ceccato, P., Flasse, S., Tarantola, S., Jacquemoud, S., Grégoire, J.-M., 2001. Detecting vegetation leaf water content using reflectance in the optical domain. Remote Sens. Environ. 77, 22–33.

Chen, Y., Romps, D.M., Seeley, J.T., Veraverbeke, S., Riley, W.J., Mekonnen, Z.A., Randerson, J.T., 2021. Future increases in Arctic lightning and fire risk for permafrost carbon. Nat. Clim. Chang. 11, 404–410.

De Jeu, R.A.M., Owe, M., 2003. Further validation of a new methodology for surface moisture and vegetation optical depth retrieval. Int. J. Remote Sens. 24, 4559–4578.

Dickinson, M.B., Dietenberger, M., Ellicott, E.A., Hardy, C., Hudak, A.T., Kremens, R., Mathews, W., Schroeder, W., Smith, A.M., Strand, E.K. (2016). The use of remotely-sensed wildland fire radiation to infer the fates of carbon during biomass combustion - the need to understand and quantify a fire's mass and energy budget. In (pp. B21M-06).

Dissing, D., Verbyla, D.L., 2003. Spatial patterns of lightning strikes in interior Alaska and their relations to elevation and vegetation. Can. J. For. Res. 33, 770–782.

ECCC (2022). Environment and Climate Change Canada Historical Hydrometric Data web site, <https://wateroffice.ec.gc.ca/mainmenu/historical_data_index_e.html>, Accessed on 2022.08.25.

Flannigan, M., 2015. Fire evolution split by continent. Nat. Geosci. 8, 167–168.

GMAO (2015). Goddard Space Flight Center Distributed Active Archive Center (GSFC DAAC). In G.M.a.A.O. (GMAO) (Ed.). Greenbelt, MD, USA:: Goddard Space Flight Center Distributed Active Archive Center (GSFC DAAC).

Hersbach, H., Bell, B., Berrisford, P., Biavati, G., Horányi, A., Muñoz Sabater, J., Nicolas, J., Peubey, C., Radu, R., Rozum, I., Schepers, D., Simmons, A., Soci, C., Dee, D., Thépaut, J-N. (2018). ERA5 hourly data on single levels from 1959 to present. Copernicus Climate Change Service (C3S) Climate Data Store (CDS). In H. Hersbach, Bell, B., Berrisford, P., Biavati, G., Horányi, A., Muñoz Sabater, J., Nicolas, J., Peubey, C., Radu, R., Rozum, I., Schepers, D., Simmons, A., Soci, C., Dee, D., Thépaut, J-N. (Ed.).

Hessilt, T.D., Abatzoglou, J.T., Chen, Y., Randerson, J.T., Scholten, R.C., van der Werf, G., Veraverbeke, S., 2022. Future increases in lightning ignition efficiency and wildfire occurrence expected from drier fuels in boreal forest ecosystems of western North America. Environ. Res. Lett. 17, 54008.

Jones, M.W., Abatzoglou, J.T., Veraverbeke, S., Andela, N., Lasslop, G., Forkel, M., Smith, A.J.P., Burton, C., Betts, R.A., van der Werf, G.R., Sitch, S., Canadell, J.G., Santín, C., Kolden, C., Doerr, S.H., Le Quéré, C., 2022. Global and regional trends and drivers of fire under climate change. Rev. Geophys. 60, e2020RG000726.

Kalashnikov, D.A., Abatzoglou, J.T., Nauslar, N.J., Swain, D.L., Touma, D., Singh, D., 2022. Meteorological and geographical factors associated with dry lightning in central and northern California. Environmental Research: Climate 1, 025001.

Kerr, Y., Waldteufel, P., Richaume, P., Davenport, I., Ferrazoli, P., Wigneron, J.-P., 2019. Algorithm Theoretical Basis Document (ATBD) for the SMOS Level 2 Soil Moisture Processor Development Continuation Project, vol. SO-TN-ARG-L2PP-0037. CESBIO, SM-ESL, CBSA, Toulouse, France.

Kerr, Y.H., Waldteufel, P., Richaume, P., Wigneron, J.P., Ferrazzoli, P., Mahmoodi, A., Bitar, A.A., Cabot, F., Gruhier, C., Juglea, S.E., Leroux, D., Mialon, A., Delwart, S., 2012. The SMOS soil moisture retrieval algorithm. IEEE Trans. Geosci. Remote Sens. 50, 1384–1403.

Kirshbaum, D., Wang, C.-C., 2014. Boundary layer updrafts driven by airflow over heated terrain. J. Atmos. Sci. 71.

Kochtubajda, B., Stewart, R.E., Flannigan, M.D., Bonsal, B.R., Cuell, C., Mooney, C.J., 2019. An assessment of Surface and atmospheric conditions associated with the extreme 2014 wildfire season in Canada's Northwest Territories. Atmos. Ocean 57, 73–90.

Kustas, W.P., Norman, J.M., 1997. A two-source approach for estimating turbulent fluxes using multiple angle thermal infrared observations. Water Resour. Res. 33, 1495–1508.

Lareau, N.P., Nauslar, N.J., Abatzoglou, J.T., 2018. The Carr fire vortex: a case of pyrotornadogenesis? Geophys. Res. Lett. 45.

Leblon, B., 2005. Monitoring Forest fire danger with remote sensing. Nat. Hazards 35, 343–359.

Leblon, B., Bourgeau-Chavez, L., & San-Miguel-Ayanz, J. (2012). Use of Remote Sensing in Wildfire Management. In C. Sime (Ed.), *Sustainable Development* (p. Ch. 3). Rijeka: IntechOpen.

Lee, J.H., 2018. The consecutive dry days to trigger rainfall over West Africa. J. Hydrol. 556, 934–943.

Lee, J.H., 2021. Prediction of Large-scale wildfires with the canopy stress index derived from soil moisture active passive. IEEE J. Sel. Top. Appl. Earth Obs. Remote Sens. 14, 2096–2102.

Link, M., Entekhabi, D., Jagdhuber, T., Ferrazzoli, P., Guerriero, L., Baur, M., Ludwig, R. (2018). Vegetation Effects on Covariations of L-Band Radiometer and C-Band/L-Band Radar Observations. In, *IGARSS 2018 - 2018 IEEE International Geoscience and Remote Sensing Symposium* (pp. 357-360).

Liu, N., Lei, J., Gao, W., Chen, H., Xie, X., 2021. Combustion dynamics of large-scale wildfires. Proc. Combust. Inst. 38, 157–198.
Liu, Y., Yang, Y., Yue, X., 2018. Evaluation of satellite-based soil moisture products over four different continental in-situ measurements. Remote Sens. (Basel) 10, 1161.
Luan, X., Vico, G., 2021. Canopy temperature and heat stress are increased by compound high air temperature and water stress and reduced by irrigation – a modeling analysis. Hydrol. Earth Syst. Sci. 25, 1411–1423.
McArthur, A.G., Cheney, N.P., 2015. The Characterization of fires in relation to ecological studies. Fire Ecology 11, 3–9.
Meyer, T., Weihermüller, L., Vereecken, H., Jonard, F. (2018). Vegetation Optical Depth and Soil Moisture Retrieved from L-Band Radiometry over the Growth Cycle of a Winter Wheat. In, *Remote Sensing*.
Moore, P.F., 2019. Global Wildland Fire Management Research Needs. Curr Forestry Rep 5, 210–225. https://doi.org/10.1007/s40725-019-00099-y.
Morgenstern, D., Stucke, I., Simon, T., Mayr, G.J., Zeileis, A., 2022. Differentiating lightning in winter and summer with characteristics of the wind field and mass field. Weather Clim. Dynam. 3, 361–375.
Muñoz Sabater, J. (2021). ERA5-Land hourly data from 1950 to 1980. Copernicus Climate Change Service (C3S) Climate Data Store (CDS). In J. Muñoz Sabater (Ed.).
Myneni, R., Y. Knyazikhin, T. Park. (2015). MCD15A2H MODIS/Terra+Aqua Leaf Area Index/FPAR 8-day L4 Global 500m SIN Grid V006. In R. Myneni, Y. Knyazikhin, T. Park. (Ed.): NASA EOSDIS Land Processes DAAC.
Nauslar, N.J., Abatzoglou, J.T., Marsh, P.T., 2018. The 2017 North Bay and Southern California fires: a case study. In, Fire.
Nolan, R.H., Resco de Dios, V., Boer, M.M., Caccamo, G., Goulden, M.L., Bradstock, R.A., 2016. Predicting dead fine fuel moisture at regional scales using vapour pressure deficit from MODIS and gridded weather data. Remote Sens. Environ. 174, 100–108.
Oehri, J., Schaepman-Strub, G., Kim, J.-S., Grysko, R., Kropp, H., Grünberg, I., Zemlianskii, V., Sonnentag, O., Euskirchen, E.S., Reji Chacko, M., Muscari, G., Blanken, P.D., Dean, J.F., di Sarra, A., Harding, R.J., Sobota, I., Kutzbach, L., Plekhanova, E., Riihelä, A., Boike, J., Miller, N.B., Beringer, J., López-Blanco, E., Stoy, P.C., Sullivan, R.C., Kejna, M., Parmentier, F.-J.-W., Gamon, J.A., Mastepanov, M., Wille, C., Jackowicz-Korczynski, M., Karger, D.N., Quinton, W.L., Putkonen, J., van As, D., Christensen, T.R., Hakuba, M.Z., Stone, R.S., Metzger, S., Vandecrux, B., Frost, G.V., Wild, M., Hansen, B., Meloni, D., Domine, F., te Beest, M., Sachs, T., Kalhori, A., Rocha, A.V., Williamson, S.N., Morris, S., Atchley, A.L., Essery, R., Runkle, B.R.K., Holl, D., Riihimaki, L.D., Iwata, H., Schuur, E.A.G., Cox, C. J., Grachev, A.A., McFadden, J.P., Fausto, R.S., Göckede, M., Ueyama, M., Pirk, N., de Boer, G., Bret-Harte, M.S., Leppäranta, M., Steffen, K., Friborg, T., Ohmura, A., Edgar, C.W., Olofsson, J., Chambers, S.D., 2022. Vegetation type is an important predictor of the arctic summer land surface energy budget. Nat. Commun. 13, 6379.
O'Neill, P.E., Chan, S., Njoku, E.G., Jackson, T., Bindlish, R., Chaubell, J., Colliander, A., 2021. SMAP enhanced L3 radiometer global and Polar grid daily 9 km EASE-grid soil moisture. In: O'Neill, P.E., Chan, S., Njoku, E.G., Jackson, T., Bindlish, R., Chaubell, J., Colliander, A. (Eds.), Boulder. NASA National Snow and Ice Data Center Distributed Active Archive Center, Colorado USA.
Orville, R.E., Huffines, G.R., Burrows, W.R., Cummins, K.L., 2011. The north American lightning detection network (NALDN)—analysis of flash data: 2001–09. Mon. Weather Rev. 139, 1305–1322.
Pirotti, F., Adedipe, O., Leblon, B. (2023). Sentinel-1 Response to Canopy Moisture in Mediterranean Forests before and after Fire Events. In, *Remote Sensing*.
Parks, S., Parisien, M.-A., Miller, C., Dobrowski, S., 2014. Fire Activity and Severity in the Western US Vary along Proxy Gradients Representing Fuel Amount and Fuel Moisture. PLoS One 9, e99699.
Reul, N., Chapron, B., Zabolotskikh, E., Donlon, C., Quilfen, Y., Guimbard, S., Piolle, J.F., 2016. A revised L-band radio-brightness sensitivity to extreme winds under tropical cyclones: the five year SMOS-storm database. Remote Sens. Environ. 180, 274–291.
Reul, N., Tenerelli, J., Chapron, B., Vandemark, D., Quilfen, Y., Kerr, Y., 2012. SMOS satellite L-band radiometer: A new capability for ocean surface remote sensing in hurricanes. Journal of Geophysical Research: Oceans 117.
Rogers, B.M., Soja, A.J., Goulden, M.L., Randerson, J.T., 2015. Influence of tree species on continental differences in boreal fires and climate feedbacks. Nat. Geosci. 8, 228–234.
Schultz, C.J., Nauslar, N.J., Wachter, J.B., Hain, C.R., Bell, J.R., 2019. Spatial. Temporal and Electrical Characteristics of Lightning in Reported Lightning-Initiated Wildfire Events, Fire, p. 2.
Szpakowski, D.M., Jensen, J.L.R., 2019. A review of the applications of remote sensing in fire ecology. In, Remote Sensing.
Taylor, C.M., Gounou, A., Guichard, F., Harris, P.P., Ellis, R.J., Couvreux, F., De Kauwe, M., 2011. Frequency of sahelian storm initiation enhanced over mesoscale soil-moisture patterns. Nat. Geosci. 4, 430–433.
Taylor, C.M., de Jeu, R.A.M., Guichard, F., Harris, P.P., Dorigo, W.A., 2012. Afternoon rain more likely over drier soils. Nature 489, 423–426.
van Wagner, C.E. (1987). Development and structure of the Canadian Forest Fire Weather Index System. In F.T. Report (Ed.), *Forestry Technical Report* (p. 35). Headquarters, Ottawa.
Veraverbeke, S., Rogers, B.M., Goulden, M.L., Jandt, R.R., Miller, C.E., Wiggins, E.B., Randerson, J.T., 2017. Lightning as a major driver of recent large fire years in north American boreal forests. Nat. Clim. Chang. 7, 529–534.
Walker, X.J., Rogers, B.M., Baltzer, J.L., Cumming, S.G., Day, N.J., Goetz, S.J., Johnstone, J.F., Schuur, E.A.G., Turetsky, M.R., Mack, M.C., 2018. Cross-scale controls on carbon emissions from boreal forest megafires. Glob. Chang. Biol. 24, 4251–4265.
Walker, X.J., Baltzer, J.L., Cumming, S.G., Day, N.J., Ebert, C., Goetz, S., Johnstone, J.F., Potter, S., Rogers, B.M., Schuur, E.A.G., Turetsky, M.R., Mack, M.C., 2019. Increasing wildfires threaten historic carbon sink of boreal forest soils. Nature 572, 520–523.
Wang, J., Strong, K. (2019). *British Columbia's forest fires, 2018*. Statistics Canada.
Wang, J., Chagnon, F.J.F., Williams, E.R., Betts, A.K., Renno, N.O., Machado, L.A.T., Bisht, G., Knox, R., Bras, R.L., 2009. Impact of deforestation in the Amazon basin on cloud climatology. Proc. Natl. Acad. Sci. 106, 3670–3674.
Wang, H., Wigneron, J.-P., Ciais, P., Yao, Y., Fan, L., Liu, X., Li, X., Green, J.K., Tian, F., Tao, S., Li, W., Frappart, F., Albergel, C., Wang, M., Li, S., 2023. Seasonal variations in vegetation water content retrieved from microwave remote sensing over Amazon intact forests. Remote Sens. Environ. 285, 113409.
Wells, J.V., Dawson, N., Culver, N., Reid, F.A., Morgan Siegers, S., 2020. The state of conservation in North America's boreal Forest: issues and opportunities. Frontiers in Forests and Global Change 3.
Wigneron, J.P., Jackson, T.J., O'Neill, P., De Lannoy, G., de Rosnay, P., Walker, J.P., Ferrazzoli, P., Mironov, V., Bircher, S., Grant, J.P., Kurum, M., Schwank, M., Munoz-Sabater, J., Das, N., Royer, A., Al-Yaari, A., Al Bitar, A., Fernandez-Moran, R., Lawrence, H., Mialon, A., Parrens, M., Richaume, P., Delwart, S., Kerr, Y., 2017. Modelling the passive microwave signature from land surfaces: a review of recent results and application to the L-band SMOS & SMAP soil moisture retrieval algorithms. Remote Sens. Environ. 192, 238–262.
Yebra, M., Dennison, P.E., Chuvieco, E., Riaño, D., Zylstra, P., Hunt, E.R., Danson, F.M., Qi, Y., Jurdao, S., 2013. A global review of remote sensing of live fuel moisture content for fire danger assessment: moving towards operational products. Remote Sens. Environ. 136, 455–468.
Yebra, M., Dennison, P.E., Chuvieco, E., Riaño, D., Zylstra, P., Hunt, E.R., Danson, F.M., Qi, Y., Jurdao, S., 2013. A global review of remote sensing of live fuel moisture content for fire danger assessment: Moving towards operational products. Remote Sensing of Environment 136, 455–468.
Yebra, M., Shokirov, S., Leavesley, A., & Kristina, A. (2022). Validation of a high-resolution fuel moisture content product for Australia.
Zhang, Y., Fan, J., Logan, T., Li, Z., Homeyer, C.R., 2019. Wildfire impact on environmental thermodynamics and severe convective storms. Geophys. Res. Lett. 46, 10082–10093.